Hingepoints and neural folds reveal conserved features of primary neurulation in the zebrafish forebrain

Jonathan M. Werner[1], Maraki Y. Negesse[1], Dominique L. Brooks[1], Allyson R. Caldwell[1], Jafira M. Johnson[1] and Rachel Brewster[1]

1. Department of Biological Sciences, University of Maryland Baltimore County, Baltimore, MD 21250

ABSTRACT

Primary neurulation is the process by which the neural tube, the central nervous system precursor, is formed from the neural plate. Incomplete neural tube closure occurs frequently, yet underlying causes remain poorly understood. Developmental studies in amniotes and amphibians have identified hingepoint and neural fold formation as key morphogenetic events and hallmarks of primary neurulation, the disruption of which causes neural tube defects. In contrast, the mode of neurulation in teleosts like zebrafish has remained highly debated. Teleosts are thought to have evolved a unique pattern of neurulation, whereby the neural plate infolds in absence of hingepoints and neural folds, at least in the hindbrain/trunk where it has been studied. We report here on zebrafish forebrain morphogenesis where we identify these morphological landmarks. Our findings reveal a deeper level of conservation of neurulation than previously recognized and establish the zebrafish as a model to understand human neural tube development.

INTRODUCTION

Primary neurulation is the process by which the neural tube, the precursor of the brain and spinal cord, is shaped from an open single-cell layered epithelium, known as the neural plate. These morphogenetic events have mostly been studied in amniotes (mouse and chick) and amphibians (frogs), where conserved mechanisms were identified. Following neural induction, the neural plate (Figure 1A) narrows and elongates by convergent extension movements [1,2]. The morphology of the neural plate is further changed by bending in a biphasic manner, initiated at hingepoints [3]. The first morphological event is the formation of the medial hingepoint (MHP), which bends the flat neural plate into a V shape, forming the neural groove (Figure 1B). Neural folds at the edges of the neural plate are subsequently elevated by this neuroectoderm-intrinsic force and also by the expansion of the head mesoderm in the cranial region [4]. In the second phase, the neural plate bends and folds at paired dorso-lateral hingepoints (DLHPs), which brings the neural folds closer together (Figure 1C). The neural folds eventually meet and fuse at the dorsal midline, completing neural tube formation. The dorsal midline is subsequently remodeled to separate the inner neuroectoderm from the outer non-neural ectoderm fated to become the epidermis (Figure 1D). In the cranial region of amniotes, neural tube closure is initiated at several sites and extends via a zippering process either in a unidirectional or bidirectional manner from these closure points to seal the neural tube. Incomplete cranial neural tube closure occurs frequently, resulting in anencephaly and exencephaly [3].

Several cellular mechanisms have been identified that contribute to the bending of the neural plate, among which apical constriction is the most studied [5-8]. A meshwork of F-actin accumulates at the apical cortex of neuroectodermal cells and contracts, thereby reducing

55 the cell apex during neural tube closure (Figure 1b1). The contraction is driven by the
56 molecular motor myosin that co-localizes with F-actin at the apical cortex. Disruption of F-
57 actin using drug inhibitors or in mice deficient for regulators of the cytoskeleton such as
58 Shroom3, the actin-binding protein vinculin or a RhoA-specific GEF (GEF-H1) causes severe
59 cranial neural tube defects [5,9-14]. Similarly, treatment with blebbistatin, an inhibitor of non-
60 muscle myosin II activity, impairs apical constriction of hingepoint cells in the superficial layer
61 of the *Xenopus* neural plate [15].

62 In contrast to hingepoint formation, the cell intrinsic mechanisms that shape neural fold
63 cells are less understood. The neural folds are bilaminar, consisting of a layer of
64 neuroectoderm capped by a layer of non-neural ectoderm [16]. Neural fold fusion involves the
65 formation of cellular protrusions (filopodia and lamellipodia) that span the midline gap and
66 establish the first contact and attachment points with neural fold cells from the contralateral
67 side [17-19] (Figure 1c1). There is little consensus on the cell type, neuroectoderm or non-neural
68 ectoderm, that generates the cellular protrusions as it varies depending on the species and
69 the axial level. In the mouse forebrain, the initial contact is made by neuroectodermal cells
70 [17,20-23]. Treatment with Cytochalasin D, an inhibitor of actin polymerization or genetic ablation
71 of the cytoskeletal regulators Rac1 or Cdc42 blocks the formation of protrusions and prevents
72 neural fold fusion [19], revealing the central role of these cellular processes.

73 Though more anterior regions of the neural tube undergo primary neurulation as
74 described above, most vertebrates also exhibit a distinct type of neural tube formation in
75 more posterior regions, termed secondary neurulation. During this process, a mesenchymal
76 cell population condenses into a solid neural rod that subsequently epithelializes and forms a
77 central lumen [24,25]. The mechanisms of neural tube formation in zebrafish have been the

source of considerable debate, and it has been proposed that they are unique among vertebrates [26 27]. In zebrafish, the neural tube in the hindbrain and trunk region initially forms a solid rod (the neural keel) that later develops a lumen, a process seemingly analogous to secondary neurulation [28]. However, examination of the tissue architecture in zebrafish [29-31] and other teleosts [32,33] revealed that the neural rod is shaped by infolding of a neural plate (albeit incompletely epithelialized), which best fits the description of primary neurulation [26]. Despite this evidence, differences in tissue architecture, the mesenchymal-like character of the neural plate and the apparent lack of hingepoints, neural groove and neural folds are difficult to reconcile with a mode of primary neurulation and have contributed to the persistent view that neural tube formation in teleosts is different than in other vertebrates [34-36].

We show here that, in contrast to the zebrafish hindbrain and trunk region, the process of neural tube formation in the forebrain of this teleost exhibits the hallmarks of primary neurulation observed in other vertebrates. We observe the presence of hingepoints and neural folds in the epithelialized anterior neural plate (ANP), demonstrate that formation of the MHP involves oscillatory apical contractions that progressively reduce the apical surface, and show that disruption of myosin function impairs apical constriction of these cells and neural fold convergence. We further show that neural tube closure is initiated at two separate sites in the forebrain and that fusion of the neural folds is mediated by filopodial-like extensions of neuroectodermal cells that bridge the midline. These findings identify conserved mechanisms of primary neurulation that were previously overlooked in teleosts and support the suitability of zebrafish for understanding the etiology of human neural tube defects.

RESULTS

Epithelial character of the anterior neural plate is associated with bending and folding movements

The zebrafish ANP is quite distinct from the neural plate in more posterior regions, as it undergoes precocious epithelialization [37]. To assess whether the epithelialized nature of the ANP also correlates with a change in the mode of neurulation, we examined the morphology of the neuroectoderm in optical cross sections at developmental stages ranging from 2 to 7 somites (som). We observed that at 2-5 som the ANP has a V shape marked by a medial neural groove (black arrowhead) flanked by the elevated lateral edges of the ANP (white arrowhead), which are reminiscent of neural folds (Figure 2A-C). By 6 som the groove is no longer visible and the elevated edges of the ANP have fused medially (Figure 2E, white arrowhead) and form a dorsal bulge by 7 som (Figure 2F, white arrowhead). These observations suggest that the ANP bends and folds around hingepoints to facilitate the medial convergence and fusion of neural folds at the dorsal midline.

The anterior neural plate is multi-layered and gives rise to the eyes and forebrain

The central part of the ANP is fated to become the eyes, while its lateral edges produce the dorsally-located telencephalon and the ventral-most ANP region gives rise to the hypothalamus/ventral diencephalon [37,38]. To gain a better understanding of the morphogenetic events that shape the zebrafish ANP, we examined transverse views of transgenic Tg[*emx3:YFP*] embryos at developmental stages 2, 5, 7 and 10 som, in which telencephalon precursors are labeled with the yellow fluorescent protein (YFP) [39]. We observed, as previously described [37], that the ANP is a multi-layered tissue, with a

123 mesenchymal superficial core and a marginal or deep layer. These layers will henceforth be
124 referred to as the superficial and deep layers, respectively (s and d in Figure 3A,B). The YFP-
125 positive lateral edges of the ANP elevate, migrate over the eye field and fuse medially at 7
126 som to form the telencephalon (Figure 3C-D) [37,38]. By 7 som the multilayered ANP (Figure
127 3A, B) resolves into a single-cell layered neuroectoderm and Ivanovitch et al. (2013)[37] have
128 shown that this process involves radial intercalation of superficial cells between deep
129 marginal cells, which also contributes to the expansion of the optic vesicles (Figure 3F, G).
130 While the morphological changes and cellular dynamics that form the eyes are quite well
131 understood [37,38], the accompanying events that shape the forebrain are for the most part
132 unknown and the focus of the current study.
133

134 **Structures analogous to hingepoints and neural folds are present in the anterior neural**
135 **plate**

136 To investigate whether the ANP bends and folds around hingepoints to bring neural folds in
137 close apposition, we examined the cytoarchitecture of this tissue in embryos at stages 2-10
138 som, labeled with phalloidin (filamentous (F) actin), anti-Sox3 (neural cells) and anti-p63
139 (epidermal cells, nuclear label) (Figure 3E-H).

140 We found that at 2 som, neural cells appear mesenchymal with no visible polarized
141 enrichment of F-actin (Figure 3E), consistent with previous observations [37]. The epidermis at
142 this stage is in a far lateral position (white arrowhead in Figure 3E).

143 Between 2 and 5 som, cells undergo rapid epithelialization, as evidenced by foci of F-
144 actin enrichment in the medial/superficial region (M in Figure 3F, I) and in two dorso-lateral
145 clusters in the deep marginal layer (DL in Figure 3F, I). The apical surfaces of the

146 epithelialized superficial cells appear to constrict and orient towards the midline, resulting in
147 the formation of a medial neural groove (asterisk in Figure 3I). Similarly, the paired dorso-
148 lateral clusters of epithelialized cells in the deep layer are also apically constricted and the
149 neuroectoderm bends and folds sharply at this level (red arrows in Figure 3I), elevating the
150 lateral edges of the ANP above the superficial layer and bringing them closer to the midline.
151 These data suggest that the medial and dorso-lateral cells enriched for apical F-actin may
152 function as hingepoints. Similarly to amphibians whose neural plate is bilayered [40], the
153 putative medial hingepoint in the zebrafish ANP forms in the superficial layer and is therefore
154 more dorsally positioned than its chick and mouse counterpart. However, the zebrafish dorso-
155 lateral hingepoints form in the deep layer.

156 The lateral edges of the ANP are bilaminar at 5 som, consisting of a layer of
157 neuroectoderm cells capped by a layer of p63-positive non-neural ectoderm (and Sox3/p63-
158 negative olfactory placodal cells bridging the two layers), indicative of a neural fold structure
159 (Figure 3F, I). The YFP-positive ANP cells in Tg[*emx3:YFP]* embryos correspond to the
160 neuroectoderm component of neural fold (Figure 3B), revealing that the tip of the neural fold
161 gives rise to the telencephalon. At 4 som, the YFP-positive region of Tg[*emx3:YFP*] embryos
162 extends the length of the forebrain (Figure 2C), delineating the anterior-posterior range of the
163 neural folds.

164 The neural fold and putative hingepoints are transient as they are no longer observed
165 in 7 som embryos. By this stage, the tips of the neural folds have converged medially and
166 fused, forming the telencephalon (Figure 3G). These cells are enriched for apical F-actin at
167 10 som, indicating that they epithelialize (Figure 3D). The non-neural ectoderm still occupies
168 a lateral position at 7 som (Figure 3C, arrowheads), however by 10 som these cells migrate

169 and fuse dorsally (single arrowhead in Figure 3D), indicating that, as observed in mice, the
170 neuroectodermal component of the neural folds meet first (Figure 1) [20,21]. Measurements of
171 the distance between the medial-most p63-positive domain and the dorsal midline at stages
172 2-7 som indicate that the non-neural ectoderm portion of the neural folds converges steadily
173 towards the midline and may provide a lateral force that contributes to the displacement of
174 neural folds (Figure 3J).

175 These observations reveal that transient medial and dorso-lateral epithelialized cell
176 clusters may be the functional equivalents of the MHP and paired DLHPs of amniotes (and
177 will be referred to henceforth as such), as they form at the right time and place to contribute
178 to the formation of the neural groove (MHP), bending of the neuroectoderm and medial
179 convergence of the neural folds (DLHPs).

180

181 **Cell shape changes underlying DLHP and neural fold formation**

182 To capture the dynamics of neural fold formation and image neuroectodermal cells at higher
183 resolution, we mosaically expressed membrane-targeted GFP (mGFP) and imaged embryos
184 at the 2-10 som stages in transverse sections (Figure 4). 3D reconstructions of some of these
185 images were generated to gain a better understanding of the spatial relation between labeled
186 cells and image cellular protrusions in multiple planes (Supplemental Figures 1, 2).

187 At 2 som, cells in the deep layer have a columnar shape with one end in contact with
188 the basal lamina and a future apical surface oriented towards the midline (Figure 4A). These
189 cells extend membrane protrusions into the superficial layer, which may promote radial
190 intercalation (inset in Figure 4A).

191 At 5 som, cells in the dorso-lateral deep layer have undergone apical constriction and
192 basal expansion, forming DLHPs (yellow dotted circles and double arrowheads in Figure
193 4B,b1; Supplemental Figure 1). These cell shape changes may initiate the outpocketing of
194 the optic vesicles (ov in Figure 4B,b1). The bilaminar organization of the neural folds is
195 clearly visible at this stage. Neuroectoderm cells within the neural folds (arrows in Figure 3b1
196 and c1) are elongated and their basal poles are constricted, which gives them the
197 appearance of fanning out from a focal point (red circles in Figure 4b1 and c1) that spatially
198 coincides with a sharp bend in the neuroectoderm. The plasma membrane at the future
199 apical surface of these cells is ruffled, indicative of dynamic protrusive activity (Supplemental
200 Figure 2).

201 By 7 som (Figure 4D, Supplemental Figure 2), neuroectoderm cells of the neural folds
202 have elongated and reached the dorsal midline. They maintain their earlier organization with
203 basal poles constricted and clustered at a focal point on the basement membrane (red circle
204 in Figure 4d1). 3D reconstructions reveal that these cells are finger-shaped as they extend
205 across the dorsal midline. DLHP cells maintain their apical constriction/basal expansion and
206 further elongate, contributing to the expansion of the optic vesicles (dotted double arrowhead
207 in Figure 4d1).

208 At 10 som (Figure 4E, e1) deep cells in the eye field and neural folds have a columnar,
209 epithelial organization. Consistent with previous findings, eye field cells shorten along their
210 apico-basal axis by contracting their apical processes and coincidently transition to a more
211 dorso-ventral orientation [37] (dotted double arrow in Figure 4e1). Cuboidal non-neural
212 ectoderm cells cover the dorsal surface of the newly formed telencephalon (arrowheads in
213 Figure 4e1.

214 The dynamic cell shape changes in the deep layer of the neuroectoderm were
215 quantified by measuring cell length and the apico:basal ratio of mGFP-labeled cells located at
216 different positions along the medio-lateral axis of the ANP at 2, 5 and 7 som (Figure 5).
217 These data reveal that the average length of DLHP cells increases while their apical:basal
218 ratio decreases between 2 and 7 som, coincident with optic vesicle evagination. They also
219 confirm that neuroectoderm cells of the neural folds elongate and adopt the reverse
220 configuration, with basally constricted poles.
221 These findings indicate that zebrafish DLHP cells adopt a wedge shape similar to the
222 cytoarchitecture of DLHPs in amphibians and amniotes, which enables epithelial bending.
223 They further identify basal constriction of neuroectodermal cells in the neural folds as a cell
224 shape change that contributes to neural fold formation.
225
226 **MHP cells constrict apically and elongate**
227 While mosaic expression of mGFP enabled high resolution imaging of DLHPs and neural
228 folds, it resulted in few cells labeled in the medial superficial layer, where the MHP forms.
229 Phalloidin labeling was therefore used to image these cells in 2 and 5 som embryos.
230 At the 2 som stage, some but not all medial/superficial cells immediately below the
231 enveloping layer (EVL) are apically constricted, forming the MHP (Figure 6A-a2). By 5 som,
232 MHP cells appear more densely packed, the majority of them are apically constricted and
233 oriented towards the midline. Concomitant with these cell shape changes and the medial
234 convergence of neural folds, MHP cells shift to a more ventral position (Figure 6B-b2. A small
235 opening, the neural groove, is observed immediately above the MHP at this stage (NG in
236 Figure 6b1).

237 Measurements of the apico:basal surface ratio of MHP cells in 5 som embryos
238 confirmed that they are wedge-shaped (Figure 6c1). Similar to amphibians [41], apical
239 constriction appears tightly coupled to cell elongation, as the length-to-width ratio (LWR) of
240 MHP cells increases significantly between 2 and 5 som (Figure 6c2). Thus, both apical
241 constriction and cell elongation appear to shape the MHP and contribute to tissue-level
242 morphogenesis.
243 Another contributing factor to hingepoint formation in amniotes is the basal location of
244 nuclei in both the medial and lateral hingepoints [42,43]. To evaluate the relative apico-basal
245 position of DAPI-labeled nuclei in MHP cells, we measured the distance between the dorsal
246 nuclear surface and the basal pole of MHP cells as a fraction of the total cell length (Figure
247 6c3). This analysis revealed that at 2 and 5 som stages the position of the nucleus does not
248 change significantly and is therefore unlikely to contribute to wedging of this cell population.
249
250 **Oscillatory constrictions progressively reduce the apical surface of MHP cells**
251 To gain a better understanding of the dynamics of apical constriction and cell internalization,
252 the ANP of embryos ubiquitously expressing mGFP was imaged from a dorsal view using
253 time-lapse microscopy between 2 som to 4 som (n = 2 embryos, Figure 6D and Supplemental
254 Figure 3). The focal plane was set immediately below the EVL, at the level of the MHP.
255 These movies revealed clusters of medially-located cells that undergo progressive cell
256 surface reduction (color-coded in Figure 6d1-d6), while the surface area of adjacent, more
257 lateral cells remained unchanged for the duration of imaging (yellow asterisks in Figure 6d1-
258 d6). EVL cells came into focus immediately posterior to the cells with reducing apices. Since
259 the EVL is drawn inward as a result of its close contact with apically constricting MHP cells

260 (Figure 6B-b2), we surmise that apical constriction proceeds in a posterior-to-anterior
261 direction. In later movie frames, EVL cells are no longer observed within the field of view,
262 coinciding with the proximity of the neural folds to the midline (Supplemental Figure 3),
263 indicating that the medial EVL cells eventually lose contact with the MHP and return to their
264 original position, allowing the neural folds to fuse at the dorsal midline.

265 To further examine the dynamics of apical constriction, the surface area of superficial
266 ANP cells was measured at regular intervals. Cells located at the midline (MHP cells, band
267 width of 20 μm from the midline, Figure 7A, C) or immediately adjacent to the midline (MHP-
268 adjacent cells, greater than 20 μm from the midline, Figure 7B) were scored. This analysis
269 revealed that individual cells undergo pulsed contractions. Between pulses the surface area
270 of cells expands slightly, but not back to original values (Figure 7A, C), resulting in a gradual
271 decrease of pulsing amplitude over time, which is more pronounced for MHP cells than their
272 immediate neighbors.

273 Together these data indicate that MHP cells undergo progressive narrowing of their
274 apical pole via pulsed contractions and that these cellular dynamics proceed in a posterior-to-
275 anterior direction.

276

277 **Neural fold fusion is initiated at closure points and mediated by dynamic protrusive**
278 **activity**

279 In mice, neurulation proceeds unevenly along the anterior-posterior axis with multiple closure
280 initiation sites [3], raising the question of whether neural fold fusion also occurs asynchronously
281 in zebrafish. To address this, we performed time-lapse imaging of embryos mosaically
282 expressing mGFP from a dorsal view around the time when opposing neural folds approach

283 the midline (n= 2 embryos, Figure 8A and Supplemental Figure 4). Neuroectoderm cells of
284 the neural fold were identified based on their elongated shape and dorsal location (unlike
285 MHP cells they do not become internalized).

286 These movies revealed that the neural folds have an arc shape with the apex
287 positioned anteriorly (red asterisks in Figure 8A), which is strikingly similar to the expression
288 domain of the telencephalon marker *emx3* at the onset of neural fold convergence (inset in
289 Figure 8A). Neural fold fusion is initiated near the apex of the arch and proceeds in an
290 anterior-to-posterior direction for a distance of approximately 35 μm (red dotted line in Figure
291 8a3). At this level, defined as closure point one (C1 in Figure 8a2), neural fold fusion
292 proceeds asynchronously, as a second closure initiation site is formed more posteriorly (C2 in
293 Figure 8A5), defining an eye-shaped opening (white dotted oval in Figure 6 a4, a5). A
294 zippering process then begins at the anterior and posterior corners, progressing from both
295 ends toward the middle (Figure a6,a7; Supplemental Figure 4).

296 The events that complete neural fold fusion in amniotes involve the extension of
297 dynamic cellular projections towards the midline as opposing neural folds approach each
298 other [17-19]. These cellular extensions are thought to function as transient bridges that promote
299 the formation of stable intermediate closure points. Likewise, we observed that zebrafish
300 neuroectodermal cells extend filopodia across the midline to establish contact with cells from
301 the contralateral side. Furthermore, the cell bodies hyper-extend beyond the midline (Figure
302 6b3, b4 and Supplemental Figure 5), indicating that they interdigitate between neuroectoderm
303 cells of the opposing neural fold. These cellular extensions are eventually retracted, clearing
304 the midline, which coincides with the timing of epithelialization and the establishment of apical
305 junctions (Figure 3D).

306 The presence of closure points and the usage of filopodia to establish contact with
307 neural fold cells across the midline reveal additional aspects of forebrain neurulation that are
308 conserved in zebrafish.
309
310 **Molecular characteristics of medial and lateral hingepoints**
311 Key features of cells that form hingepoints include apico-basal polarization, accumulation of
312 an apical contractile machinery composed of actin filaments (F-actin) and non-muscle myosin
313 II [44]. To test whether the MHP and DLHPs in the zebrafish forebrain have some or all of these
314 characteristics and to evaluate the timing of their maturation, the localization of Pard3-GFP (a
315 marker for apical polarity, transiently expressed following mRNA injection), F-actin
316 (phalloidin) and phospho-Myosin Light Chain II (anti-P-MLC) was examined in 3, 4 and 5 som
317 embryos (Figure 9).
318 Apical co-localization of Pard3-GFP and F-actin was confirmed in both the MHP and
319 DLHPs, beginning at the 3 som stage (data not shown) and became more prominent by 4
320 and 5 som (Figure 9A-F). Thus, while the establishment of apico-basal polarity is generally
321 delayed in the zebrafish neural plate relative to amniotes, the cell clusters that undergo apical
322 constriction in the ANP are epithelialized earlier than other neural plate cells, consistent with
323 previous observations [37]. P-MLC accumulation at the apical pole is slightly delayed relative to
324 Pad3-GFP, as it is only apparent by the 5 som stage in MHP cells where it overlaps with F-
325 actin (Figure 9J-L). In contrast, P-MLC enrichment is not observed in the DLHPs (open
326 arrowhead in Figure 9K). P-MLC also accumulates in the cell cortex of all neuroectoderm
327 cells where it overlaps with F-actin, in addition to the basal surface of EVL cells (arrow in
328 Figure 9H, K) and at the interface between the neuroectoderm and non-neural ectoderm

329 (dotted line in Figure 9J-L).

330 These findings reveal that both the MHP and DLHP undergo early epithelialization and
331 accumulate F-actin at the apical cortex. However, the MHP and DLHPs are molecularly
332 distinct structures given that the latter is not enriched for P-MLC.

333

334 **Myosin contractility is required for MHP formation and neural fold convergence**

335 During neural tube closure, the actomyosin cytoskeleton is thought to be a driving force for
336 apical constriction [41]. To address a putative function for this molecular motor in mediating
337 apical constriction in zebrafish, non-muscle myosin II (NMII) was blocked using blebbistatin
338 and a translation-blocking morpholino (MO) targeting NMIIb [45] and the effect was analyzed in
339 5 som embryos. As expected, P-MLC levels were normal in blebbistatin-treated embryos
340 (since this drug blocks NMII activity but not its phosphorylation) and reduced in NMIIB-MO
341 injected embryos (Figure 10a1'', a2'', a3''). Both treatments severely disrupted apical
342 constriction, resulting in absence of a clearly defined MHP and failure of these cells to
343 elongate (Figure 10a1,a1' vs Figure 10a2, a2', a3, a3'). In contrast to superficial cells, cells in
344 the deep layer retained their elongated shape (double arrowheads in Figure 10a1 versus
345 a2,a3). Consistent with the earlier observation that the apices of DLHP cells do not
346 accumulate P-MLC, these cells retained their wedge shape and apical F-actin accumulation
347 in NMIIb MO-injected embryos (open arrowheads in Figure 10a3). These observations
348 highlight the conserved function of actomyosin in driving apical constriction in hingepoint
349 cells. The failure of MHP cells to elongate is unlikely due to the loss of cortical tension
350 proposed by Rolo et al. (2009) [15] as P-MLC is present in both the superficial and deep layers
351 of the ANP and rounded cells are restricted to the superficial layer. Another explanation is

352 that, as previously reported, apical constriction and microtubule-based cell elongation are
353 orchestrated by the same effector proteins [41], and NMII may provide feedback information on
354 the status of apical constriction in superficial cells.

355 At a morphological level, disruption of the actomyosin network causes neural tube
356 defects that trace back to impaired apical constriction and convergent extension in *Xenopus*
357 embryos [15]. To test whether myosin is similarly required for forebrain neural tube closure in
358 zebrafish, control (untreated and DMSO-treated) and blebbistatin-treated embryos were
359 labeled at the 2, 5 and 7 som stage via *in situ* hybridization using the telencephalon marker
360 *emx3* (Figure 10B) and the width of the posterior-most emx3 domain was measured (Figure
361 10C). In contrast to control embryos, neural fold convergence was impaired in blebbistatin-
362 treated embryos, beginning at the 5 som stage. It is possible that impaired convergent
363 extension or expansion of the interface between the neuroectoderm and non-neural ectoderm
364 layers of the neural folds contribute to this defect. However, failure of MHP cells to undergo
365 apical constriction is likely to be a significant underlying cause given that disruption of several
366 proteins implicated in this process, including Shroom3 [13] and GEF-H1, a RhoA-specific GEF
367 [14] cause severe neural tube closure defects.

368

369 **DISCUSSION**

370 We report here on mechanisms of forebrain morphogenesis in the zebrafish embryo and
371 reveal that this region of the brain is formed via a mode of primary neurulation, involving the
372 use of hingepoints and neural folds.

373 The zebrafish MHP and paired DLHPs form in the superficial and deep layers of the
374 eye field, respectively. The zebrafish MHP is more transient than its mammalian counterpart

375 since these cells eventually intercalate radially between deep layer cells, contributing to the
376 expansion of the eye vesicle [37]. Hingepoints are restricted to the ANP in zebrafish, however
377 they are also present in more posterior regions of the neural plate in amniotes. Despite this
378 difference, individual cells in the medial zone of the hindbrain neural plate were recently
379 shown to internalize via a myosin-dependent mechanism [46]. Such variation from the
380 organized cell clusters forming hingepoints in the forebrain region of the zebrafish could be
381 explained by the precocious epithelialization of the ANP [37]. It thus appears that there is a
382 transition from clustered internalization mediated by the MHP in the forebrain to individual cell
383 internalization in the hindbrain region.

384 A key feature of hingepoint cells is their reduced apical surface, which is in part due to
385 actomyosin contractility [13,41,47,48]. Apical constriction is thought to function as a purse string to
386 generate the force required to bring the neural folds together during cranial neurulation [49]. We
387 provide evidence that the zebrafish MHP also utilizes an actomyosin-based contractile
388 system. Assembly of this actomyosin network occurs via pulsed contractions with gradually
389 decreasing amplitude, akin to the ratchet model first proposed in *Drosophila* and *C. elegans*
390 [50-52] and later reported during neural tube closure in *Xenopus* [53]. We further show that
391 disruption of myosin impairs neural fold convergence. These observations indicate that the
392 actomyosin machinery is used across all vertebrate models of neurulation to drive cranial
393 neural tube closure.

394 In contrast to the MHP, the paired DLHPs do not require myosin to apically constrict,
395 suggesting that DLHP formation is regulated by a distinct mechanism. Consistent with this
396 observation, McShane and colleagues report that cell packing at a dorso-ventral boundary in
397 the mouse neural tube causes buckling of the neuroectoderm at the DLHPs [54]. It is possible

398 that such a mechanism also operates during zebrafish neurulation.

399 Neural folds in chick embryos form via a series of steps involving epithelial ridging,
400 kinking, delamination and apposition [16], although the cellular basis of these morphogenetic
401 events is not well understood. Elevation of the neural folds in the mouse cranial neural plate
402 is dependent on expansion of the head mesenchyme [55]. Neural folds in the zebrafish are
403 restricted to the ANP. The head mesenchyme is unlikely to play a significant mechanical role
404 in neural fold elevation in zebrafish as the mesoderm layer immediately underlying the ANP is
405 thin. We identify instead a neural fold-autonomous cell behavior, basal constriction, that may
406 contribute to the early stages of neural fold elevation in zebrafish and possibly also in
407 amniotes. Given that the neural folds converge medially, increasing the surface of apposition
408 between the neuroectoderm and non-neural ectoderm, it is possible that basal constriction is
409 transient and involves successive rows of neuroectodermal cells, akin to the epithelial rolling
410 model described by Keller and Shook [56].

411 The final step of primary neurulation involves the convergence and fusion of the neural
412 folds at the dorsal midline. Neural fold fusion is initiated at closure points in mammals and
413 birds, however their timing and the order in which these points close varies across species[57].
414 We observe two closure points in the zebrafish forebrain that form an eye-shaped opening
415 that narrows from the corners in a bidirectional manner. Fusion of the neural folds is
416 mediated by the formation of dynamic, actin-rich cellular protrusions that span the midline
417 and establish the first points of contact with neural fold cells from the contralateral side. Akin
418 to mice [20,21], the cells that initiate contact between apposing neural folds in zebrafish derive
419 from the neuroectoderm portion of the neural folds. The protrusive ends of the
420 neuroectoderm cells interdigitate between their contralateral counterparts, forming a rod like

421 structure, the precursor of the telencephalon, which subsequently epithelializes. Once the
422 neuroectoderm cells have met and fused, non-neural ectoderm cells complete their migration
423 and fuse at the dorsal midline.
424 Together these findings have significant implications for our understanding of the
425 evolution of neurulation and the relevance of this model organism to understand human
426 neural tube development.
427

428 **METHODS**

429 **Zebrafish strains/husbandry**

430 Studies were performed using wildtype (AB) strains or *Tg(emx3:YFP)*^{b1200}[39] and embryos
431 were raised at 28.5^{o}C. All experiments were approved by the University of Maryland,
432 Baltimore County's Institutional Animal Care and Use Committee (IACUC) and were
433 performed according to national regulatory standards.
434

435 **Nucleic acid and morpholino injections**

436 Plasmids encoding membrane-targeted Green Fluorescent Protein (mGFP) (Richard
437 Harland, University of California, Berkeley, CA, USA) and *pard3:egfp*[58] were linearized with
438 NotI and transcribed using the SP6 mMESSAGE mMACHINE kit (Ambion, AM1340). For
439 ubiquitous expression of mGFP or Par3d:eGFP, 50 pg of RNA was injected into 1-cell stage
440 embryos. For mosaic expression of mGFP, 50 pg of RNA was injected into 1 or 2 of the four
441 central blastomeres at the 16-cell stage. These blastomeres have a high probability for neural
442 fate[59] and are easy to identify for reproducible injections.

443 MOs were designed and synthesized by GeneTools (Philomath, Oregon, USA) and injected
444 into 1-cell stage embryos. *mhy10*(Non-muscle Myosin IIB, EXON2-intron2) was delivered at
445 3ng per injection.
446
447 *mhy10*: 5'-CTTCACAAATGTGGTCTTACCTTGA-3′ [45]
448
449 Microinjections were performed using a PCI-100 microinjector (Harvard Apparatus, Holliston,
450 MA, USA).
451
452 **Blebbistatin treatment**
453 90% epiboly embryos were manually dechorionated in an agarose-covered petri dish with E3
454 medium. Once embryos reached the tailbud stage, they were placed into 50μM blebbistatin
455 (B0560 Sigma-Aldrich) diluted with E3 and then incubated at 28.5^{o}C. Stock solution of
456 blebbistatin was prepared with DMSO as per manufacturer's instructions. Accordingly, a
457 control group of embryos were treated with 1% DMSO diluted with E3 alongside every
458 blebbistatin trial. Once the desired developmental stage was reached (2-, 5-, or 7-som),
459 embryos were immediately fixed with 4% paraformaldehyde (PFA). As blebbistatin is light
460 sensitive, embryos were kept in the dark as much as possible until fixation.
461
462 **Fixed tissue preparations and immunolabeling**
463 Embryos were fixed in 4% PFA for 16 hours at 4°C overnight. Immunolabeling was performed
464 on whole mount embryos, which were then sectioned with a Vibratome (Vibratome 1500
465 sectioning system). Primary antibody incubation was performed for 48 hours at 4°C and
466 secondary antibody incubation for 2.5 hours at room temperature.

467 Antibodies used: Rabbit anti-GFP at 1:1000 (Invitrogen, A11122), Rabbit anti-Sox3c at
468 1:2000 (Gift from Michael Klymkowsky), Rabbit anti-P-myosin light chain at 1:50 (Cell
469 Signaling Technology, #3671S), and Mouse anti-p63 at 1:200 (Santa Cruz BioTechnology,
470 SC-8431 no longer in production). Alexa Fluorophore secondary antibodies were all used at a
471 1:1000 concentration: Goat anti-Rabbit -488, -568, -594 and Goat anti-Mouse -488, -
472 594.Alexa Fluor 488-conjugated or 594-conjugated Phalloidin (Invitrogen, A12379 and
473 A12381) at 1:250 and DAPI (Invitrogen, D1306) were used according to manufacturer's
474 instructions. Sections were mounted on glass slides using ProLong Diamond Antifade
475 Mountant (Invitrogen, P36961). *Tg(emx3:YFP)*^{b1200}embryos were immunolabeled with anti-
476 GFP to amplify the signal. mGFP and *pard3:eGFP*-injected embryos were not immunolabeled
477 with anti-GFP.
478
479 **Whole-mount *in situ*hybridization**
480 *In situ* hybridization was performed as described [60]. *emx3* riboprobe template was
481 generated by PCR amplification using cDNA from 24hpf embryos.
482
483 T7 promoter: **TAATACGACTCACTATAGGG**
484 *emx3* antisense:
485 FWD: TCCATCCATCCTTCCCCCTT
486 RVS: **TAATACGACTCACTATAGGG**GTGCTGACTGCCTTTCCTCT
487
488 DIG-labeled riboprobes were generated using 2ul of PCR template with the Roche DIG RNA
489 Labeling Kit (T7) (Sigma aldrich, SKU 11277073910)
490
491 **Whole-mount imaging**

492 Whole-mount imaging was carried out using a Zeiss Axioscope2 microscope. Embryos were
493 imaged in a 2.5% glycerol solution.
494
495 **Confocal microscopy**
496 Time-lapse microscopy was performed as previously described [61]. Embryos were imaged
497 using a Leica confocal microscope (Leica SP5 TCS 4D) at 15 sec/frame capturing <.5μm of
498 tissue. All fluorescently labeled sections were imaged using a Leica confocal microscope
499 (Leica SP5 TCS 4D).
500
501 **Data Quantification**
502 Medial-most-p63-positive-domain migration, Figure 3J: For each hemisphere of a tissue
503 section, the distance between the medial-most p63 positive nucleus and the midline was
504 manually scored. For each embryo, measurements were taken from tissue sections ranging
505 along the anterior-posterior axis of the forebrain.
506
507 Deep layer cell morphology measurements, Figure 5: Cells were manually scored from non-
508 projected z-stack images, where cellular outlines were visually determined from the mGFP
509 signal. Cells were labeled as neuroectoderm neural fold cells based on the fan-like pattern of
510 their basal projections in contact with the non-neural ectoderm. All other cells scored were
511 within the morphologically distinct eye vesicle and were labeled as eye field cells. Neural
512 ectoderm neural fold cells and eye field cells are not morphologically distinguishable at the 2
513 somitic stage and thus were not given cell type identities at that developmental stage.
514

515 Medial hinge cell morphology measurements, Figure 6C: Cells were manually scored from
516 non-projected z-stack images of the overlay between the labeled actin cytoskeleton
517 (phalloidin) and nucleus (DAPI, not shown in Figure 6) channels. Cellular outlines were
518 visually determined from the phalloidin signal. For the nuclear position measurement (Fig
519 6c3), the distance from the dorsal edge of the nucleus to the basal membrane of the cell was
520 scored and divided by the total cell length.
521
522 Cell ratcheting, Figure 7: Live movie z-stacks for the first 35 minutes (~2-4 somites, n=2) of
523 each movie were max projected and cropped so the midline of the tissue horizontally
524 bisected the image frame. The mGFP signal was then inverted and thresholded to produce a
525 binary image. Measurements for individual cell surface areas were captured using the magic
526 wand tool in ImageJ for every frame (15 seconds) until the cell left the field of view. Plotted on
527 the x-axis is the order of frame measurements (frame 0, frame 1, frame 2,...) divided by the
528 total number of frames for which that cell was scored to standardize between 0 and 1. Plotted
529 on the y-axis, the initial value of each cell's surface area was subtracted from all
530 measurements for that cell to initialize surface area's to zero. The data was binned (n=50) to
531 obtain mean measurements and confidence intervals. Cells that underwent mitosis anytime
532 during the movie were excluded. Cells were labeled as MHP if their surface area centroid
533 from the first frame (t=0) was +- 20 μm from the midline with MHP-adjacent cells being
534 labeled as such if their centroid was > +-20 μm from the midline.
535

emx3 in situ hybridization measurements, Figure 10C: The distance between the lateral edges of the posterior-most extent of the emx3 domain was manually scored for each embryo.

Statistical Analysis

The Mann-Whitney U test was used for all significance testing. The python function scipy.stats.mannwhitneyu(alternative='two-sided') was used to calculate the test statistic and P-value for each significance test. Graphs were generated using the python Seaborn package with the following functions: seaborn.boxplot(), seaborn.lmplot(), seaborn.violinplot(), seaborn.lineplot().

Data availability

The authors declare that all data supporting the findings of this study are available within the article and its supplementary information files or from the corresponding author upon reasonable request.

REFERENCES

1 Copp, A. J., Greene, N. D. & Murdoch, J. N. Dishevelled: linking convergent extension with neural tube closure. *Trends Neurosci* **26**, 453-455, doi:10.1016/S0166-2236(03)00212-1 (2003).

2 Keller, R. Shaping the vertebrate body plan by polarized embryonic cell movements. *Science* **298**, 1950-1954, doi:10.1126/science.1079478 (2002).

3 Copp, A. J., Greene, N. D. & Murdoch, J. N. The genetic basis of mammalian neurulation. *Nat Rev Genet* **4**, 784-793, doi:10.1038/nrg1181 (2003).

4 Morriss-Kay, G. M. Growth and development of pattern in the cranial neural epithelium of rat embryos during neurulation. *J Embryol Exp Morphol* **65 Suppl**, 225-241 (1981).

5 Baker, P. C. & Schroeder, T. E. Cytoplasmic filaments and morphogenetic movement in the amphibian neural tube. *Dev Biol* **15**, 432-450 (1967).

6 Sadler, T. W., Greenberg, D., Coughlin, P. & Lessard, J. L. Actin distribution patterns in the mouse neural tube during neurulation. *Science* **215**, 172-174, doi:10.1126/science.7031898 (1982).

7 Morriss-Kay, G. & Tuckett, F. The role of microfilaments in cranial neurulation in rat embryos: effects of short-term exposure to cytochalasin D. *J Embryol Exp Morphol* **88**, 333-348 (1985).

8 Schoenwolf, G. C., Folsom, D. & Moe, A. A reexamination of the role of microfilaments in neurulation in the chick embryo. *Anat Rec* **220**, 87-102, doi:10.1002/ar.1092200111 (1988).

9 Ybot-Gonzalez, P. & Copp, A. J. Bending of the neural plate during mouse spinal neurulation is independent of actin microfilaments. *Dev Dyn* **215**, 273-283, doi:10.1002/(SICI)1097-0177(199907)215:3<273::AID-AJA9>3.0.CO;2-H (1999).

10 Kinoshita, N., Sasai, N., Misaki, K. & Yonemura, S. Apical accumulation of Rho in the neural plate is important for neural plate cell shape change and neural tube formation. *Mol Biol Cell* **19**, 2289-2299, doi:10.1091/mbc.E07-12-1286 (2008).

11 Hildebrand, J. D. & Soriano, P. Shroom, a PDZ domain-containing actin-binding protein, is required for neural tube morphogenesis in mice. *Cell* **99**, 485-497 (1999).

12 Xu, W., Baribault, H. & Adamson, E. D. Vinculin knockout results in heart and brain defects during embryonic development. *Development* **125**, 327-337 (1998).

13 Haigo, S. L., Hildebrand, J. D., Harland, R. M. & Wallingford, J. B. Shroom induces apical constriction and is required for hingepoint formation during neural tube closure. *Curr Biol* **13**, 2125-2137 (2003).

14 Itoh, K., Ossipova, O. & Sokol, S. Y. GEF-H1 functions in apical constriction and cell intercalations and is essential for vertebrate neural tube closure. *J Cell Sci* **127**, 2542-2553, doi:10.1242/jcs.146811 (2014).

15 Rolo, A., Skoglund, P. & Keller, R. Morphogenetic movements driving neural tube closure in Xenopus require myosin IIB. *Dev Biol* **327**, 327-338, doi:10.1016/j.ydbio.2008.12.009 (2009).

16 Lawson, A., Anderson, H. & Schoenwolf, G. C. Cellular mechanisms of neural fold formation and morphogenesis in the chick embryo. *Anat Rec* **262**, 153-168, doi:10.1002/1097-0185(20010201)262:2<153::AID-AR1021>3.0.CO;2-W (2001).

17 Pyrgaki, C., Trainor, P., Hadjantonakis, A. K. & Niswander, L. Dynamic imaging of mammalian neural tube closure. *Dev Biol* **344**, 941-947, doi:10.1016/j.ydbio.2010.06.010 (2010).

18 Ray, H. J. & Niswander, L. A. Dynamic behaviors of the non-neural ectoderm during mammalian cranial neural tube closure. *Dev Biol* **416**, 279-285, doi:10.1016/j.ydbio.2016.06.030 (2016).

19 Rolo, A. *et al.* Regulation of cell protrusions by small GTPases during fusion of the neural folds. *Elife* **5**, e13273, doi:10.7554/eLife.13273 (2016).

20 Geelen, J. A. & Langman, J. Closure of the neural tube in the cephalic region of the mouse embryo. *Anat Rec* **189**, 625-640, doi:10.1002/ar.1091890407 (1977).

21 Geelen, J. A. & Langman, J. Ultrastructural observations on closure of the neural tube in the mouse. *Anat Embryol (Berl)* **156**, 73-88 (1979).

22 Massarwa, R., Ray, H. J. & Niswander, L. Morphogenetic movements in the neural plate and neural tube: mouse. *Wiley Interdiscip Rev Dev Biol* **3**, 59-68, doi:10.1002/wdev.120 (2014).

23 Waterman, R. E. Topographical changes along the neural fold associated with neurulation in the hamster and mouse. *Am J Anat* **146**, 151-171, doi:10.1002/aja.1001460204 (1976).

24 Criley, B. B. Analysis of embryonic sources and mechanims of development of posterior levels of chick neural tubes. *J Morphol* **128**, 465-501, doi:10.1002/jmor.1051280406 (1969).

25 Griffith, C. M., Wiley, M. J. & Sanders, E. J. The vertebrate tail bud: three germ layers from one tissue. *Anat Embryol (Berl)* **185**, 101-113 (1992).

26 Lowery, L. A. & Sive, H. Strategies of vertebrate neurulation and a re-evaluation of teleost neural tube formation. *Mech Dev* **121**, 1189-1197, doi:10.1016/j.mod.2004.04.022 (2004).

27 Andres Collazo, J. A. B., and Ray Keller. A Phylogenetic Perspective on Teleost Gastrulation. *The American Naturalist* **144**, 133-152 (1994).

28 Kimmel, C. B., Ballard, W. W., Kimmel, S. R., Ullmann, B. & Schilling, T. F. Stages of embryonic development of the zebrafish. *Dev Dyn* **203**, 253-310, doi:10.1002/aja.1002030302 (1995).

29 Papan, C. & Campos-Ortega, J. A. On the formation of the neural keel and neural tube in the zebrafishDanio (Brachydanio) rerio. *Roux Arch Dev Biol* **203**, 178-186, doi:10.1007/BF00636333 (1994).

30 Hong, E. & Brewster, R. N-cadherin is required for the polarized cell behaviors that drive neurulation in the zebrafish. *Development* **133**, 3895-3905, doi:10.1242/dev.02560 (2006).

31 Strahle, U. & Blader, P. Early neurogenesis in the zebrafish embryo. *FASEB J* **8**, 692-698, doi:10.1096/fasebj.8.10.8050667 (1994).

32 Reichenbach, A., Schaaf, P. & Schneider, H. Primary neurulation in teleosts--evidence for epithelial genesis of central nervous tissue as in other vertebrates. *J Hirnforsch* **31**, 153-158 (1990).

33 Miyayama, Y. & Fujimoto, T. Fine morphological study of neural tube formation in the teleost, Oryzias latipes. *Okajimas Folia Anat Jpn* **54**, 97-120 (1977).

34 Schmidt, R., Strahle, U. & Scholpp, S. Neurogenesis in zebrafish - from embryo to adult. *Neural Dev* **8**, 3, doi:10.1186/1749-8104-8-3 (2013).

35 Cearns, M. D., Escuin, S., Alexandre, P., Greene, N. D. & Copp, A. J. Microtubules, polarity and vertebrate neural tube morphogenesis. *J Anat* **229**, 63-74, doi:10.1111/joa.12468 (2016).

36 Yamaguchi, Y. & Miura, M. How to form and close the brain: insight into the mechanism of cranial neural tube closure in mammals. *Cell Mol Life Sci* **70**, 3171-3186, doi:10.1007/s00018-012-1227-7 (2013).

37 Ivanovitch, K., Cavodeassi, F. & Wilson, S. W. Precocious acquisition of neuroepithelial character in the eye field underlies the onset of eye morphogenesis. *Dev Cell* **27**, 293-305, doi:10.1016/j.devcel.2013.09.023 (2013).

38 England, S. J., Blanchard, G. B., Mahadevan, L. & Adams, R. J. A dynamic fate map of the forebrain shows how vertebrate eyes form and explains two causes of cyclopia. *Development* **133**, 4613-4617, doi:10.1242/dev.02678 (2006).

39 Viktorin, G., Chiuchitu, C., Rissler, M., Varga, Z. M. & Westerfield, M. Emx3 is required for the differentiation of dorsal telencephalic neurons. *Dev Dyn* **238**, 1984-1998, doi:10.1002/dvdy.22031 (2009).

40 Schroeder, T. E. Neurulation in Xenopus laevis. An analysis and model based upon light and electron microscopy. *J Embryol Exp Morphol* **23**, 427-462 (1970).

41 Suzuki, M., Morita, H. & Ueno, N. Molecular mechanisms of cell shape changes that contribute to vertebrate neural tube closure. *Dev Growth Differ* **54**, 266-276, doi:10.1111/j.1440-169X.2012.01346.x (2012).

42 Smith, J. L. & Schoenwolf, G. C. Cell cycle and neuroepithelial cell shape during bending of the chick neural plate. *Anat Rec* **218**, 196-206, doi:10.1002/ar.1092180215 (1987).

43 Smith, J. L. & Schoenwolf, G. C. Role of cell-cycle in regulating neuroepithelial cell shape during bending of the chick neural plate. *Cell Tissue Res* **252**, 491-500 (1988).

44 Lee, J. Y. & Harland, R. M. Endocytosis is required for efficient apical constriction during Xenopus gastrulation. *Curr Biol* **20**, 253-258, doi:10.1016/j.cub.2009.12.021 (2010).

45 Gutzman, J. H., Sahu, S. U. & Kwas, C. Non-muscle myosin IIA and IIB differentially regulate cell shape changes during zebrafish brain morphogenesis. *Dev Biol* **397**, 103-115, doi:10.1016/j.ydbio.2014.10.017 (2015).

46 Araya, C. *et al.* Cdh2 coordinates Myosin-II dependent internalisation of the zebrafish neural plate. *Sci Rep* **9**, 1835, doi:10.1038/s41598-018-38455-w (2019).

47 Karfunkel, P. The activity of microtubules and microfilaments in neurulation in the chick. *J Exp Zool* **181**, 289-301, doi:10.1002/jez.1401810302 (1972).

48 Lee, C., Scherr, H. M. & Wallingford, J. B. Shroom family proteins regulate gamma-tubulin distribution and microtubule architecture during epithelial cell shape change. *Development* **134**, 1431-1441, doi:10.1242/dev.02828 (2007).
49 Sawyer, J. M. *et al.* Apical constriction: a cell shape change that can drive morphogenesis. *Dev Biol* **341**, 5-19, doi:10.1016/j.ydbio.2009.09.009 (2010).
50 Martin, A. C., Kaschube, M. & Wieschaus, E. F. Pulsed contractions of an actin-myosin network drive apical constriction. *Nature* **457**, 495-499, doi:10.1038/nature07522 (2009).
51 Martin, A. C. & Goldstein, B. Apical constriction: themes and variations on a cellular mechanism driving morphogenesis. *Development* **141**, 1987-1998, doi:10.1242/dev.102228 (2014).
52 Solon, J., Kaya-Copur, A., Colombelli, J. & Brunner, D. Pulsed forces timed by a ratchet-like mechanism drive directed tissue movement during dorsal closure. *Cell* **137**, 1331-1342, doi:10.1016/j.cell.2009.03.050 (2009).
53 Suzuki, M. *et al.* Distinct intracellular Ca(2+) dynamics regulate apical constriction and differentially contribute to neural tube closure. *Development* **144**, 1307-1316, doi:10.1242/dev.141952 (2017).
54 McShane, S. G. *et al.* Cellular basis of neuroepithelial bending during mouse spinal neural tube closure. *Dev Biol* **404**, 113-124, doi:10.1016/j.ydbio.2015.06.003 (2015).
55 Zohn, I. E., Anderson, K. V. & Niswander, L. The Hectd1 ubiquitin ligase is required for development of the head mesenchyme and neural tube closure. *Dev Biol* **306**, 208-221, doi:10.1016/j.ydbio.2007.03.018 (2007).
56 Keller, R. & Shook, D. The bending of cell sheets--from folding to rolling. *BMC Biol* **9**, 90, doi:10.1186/1741-7007-9-90 (2011).
57 Nikolopoulou, E., Galea, G. L., Rolo, A., Greene, N. D. & Copp, A. J. Neural tube closure: cellular, molecular and biomechanical mechanisms. *Development* **144**, 552-566, doi:10.1242/dev.145904 (2017).
58 von Trotha, J.W., Campos-Ortega, J.A., Reugels, A.M. Apical localization of ASIP/PAR-3:EGFP in zebrafish neuroepithelial cells involves the oligomerization domain CR1, the PDZ domains, and the C-terminal portion of the protein. *Dev Dyn* **235,** 967-77 (2006).
59 Strehlow, D., Heinrich, G. & Gilbert, W. The fates of the blastomeres of the 16-cell zebrafish embryo. *Development* **120**, 1791-1798 (1994).
60 Thisse, C., Thisse, B., Schilling, T. F. & Postlethwait, J. H. Structure of the zebrafish snail1 gene and its expression in wild-type, spadetail and no tail mutant embryos. *Development* **119**, 1203-1215 (1993).
61 Jayachandran, P., Hong, E. & Brewster, R. Labeling and imaging cells in the zebrafish hindbrain. *J Vis Exp*, doi:10.3791/1976 (2010).

ACKNOWLEDGEMENTS

Funds from Howard Hughes Medical Institute through the UMBC Precollege and Undergraduate Science Education Program supported J. Werner and D. Brooks. Funds from NIH/NIGMS grants # T32-GM055036 and # R25-GM066706 and NSF LSAMP BD grant # 1500511 to UMBC supported M. Negesse. Funds from NSF LSAMP grant # 1619676 to UMBC supported J. Johnson. Funds from NIH/NIGMS MARCU*STAR T34 grant # HHS 00026 to UMBC supported D. Brooks and A. Caldwell. We thank the following people for their contributions: Tagide deCarvalho for her help with confocal imaging and image processing; Corinne Houart for the *Tg(emx3:YFP)*^{b1200} transgenic line; Jennifer Gutzman for the gift of *myh10* morpholino and Mark Van Doren for his comments on the manuscript.

AUTHOR CONTRIBUTIONS

J.W. designed and performed all experiments and carried out data analysis. M.N. identified neural fold closure points, annotated movie files and generated illustrations. D.B. and A.C. contributed to the experiments and analysis of cell polarity and myosin function. J.J. contributed to the analysis of myosin function. R.B. oversaw experimental design and analysis and wrote the manuscript.

COMPETING INTERESTS

The authors declare no competing interests

MATERIALS AND CORRESPONDENCE

Rachel Brewster

FIGURES

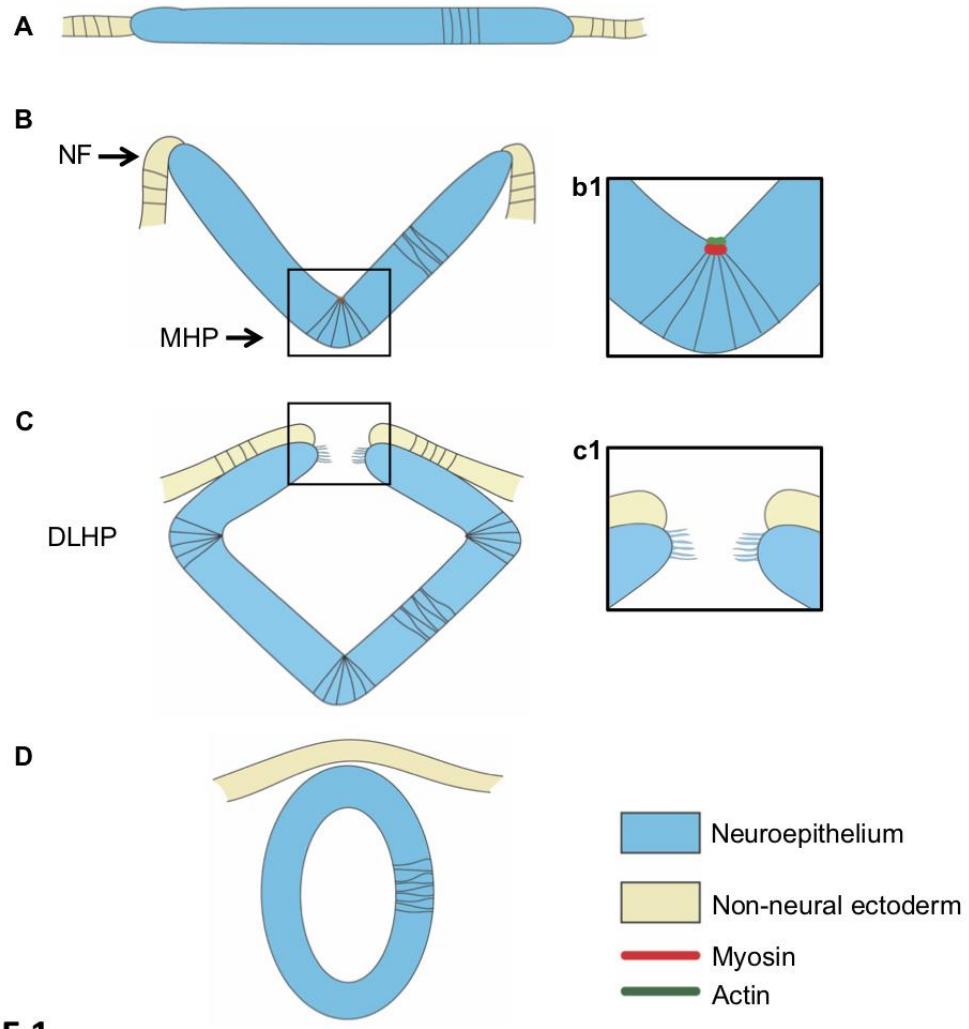

FIGURE 1

Figure 1. Neurulation in amniotes. Cross sectional illustration of stages of neurulation in amniotes. (A) The neural plate and adjacent non neural ectoderm. (B) Medial hingepoint formation shapes the neural groove and elevates the neural folds. (b1) Illustration of medial hingepoint cells that are apically-constricted and enriched for actomyosin at their apex. (C) Dorso-lateral hingepoint formation brings the neural folds in close apposition. (c1) Filopodial extensions establish contact between neural fold cells across the midline. In the mouse forebrain the first contact is established between neuroectodermal cells. (D) The neural folds fuse medially, separating the epidermis from the neural tube. Abbreviations: DLHP = dorso-lateral hingepoint; MHP = medial hingepoint; NF = neural fold.

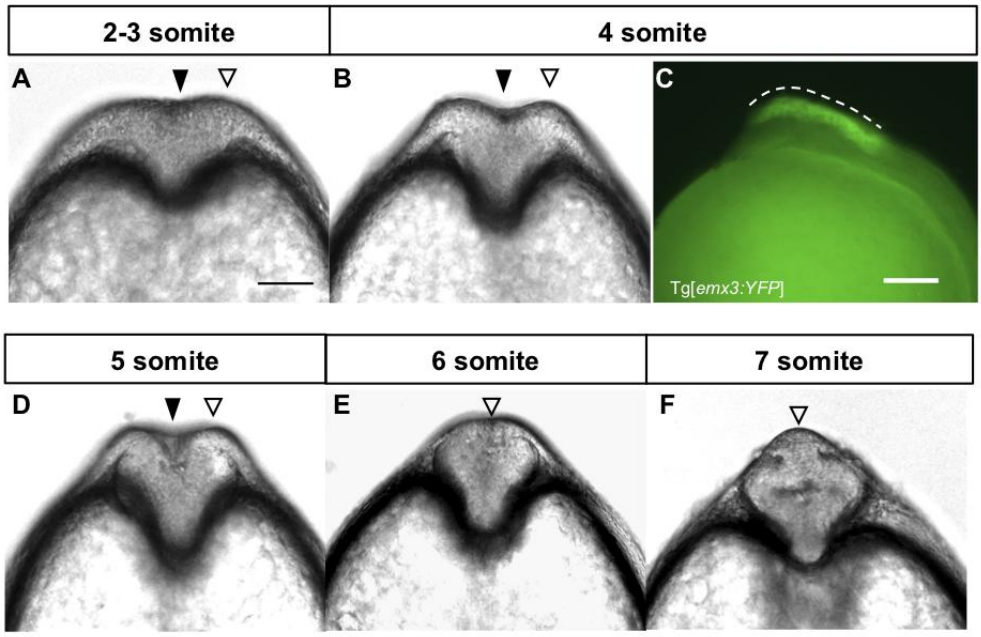

Figure 2. Presence of a neural groove and neural fold-like structures in the zebrafish forebrain. (A, B, D-F) Optical sections at the level of the forebrain of WT embryos at the 2-3 som (A), 4 som (B), 5 som (D), 6 som (E) and 7 som (F) stages. (C) Side view of a 4 som Tg[*emx3:YFP)* embryo. Annotations: black arrowhead = median groove, white open arrowhead = elevated neural-fold-like structure, dotted line = A-P range of the neural folds. Scale bars in A and C: 100 µm.

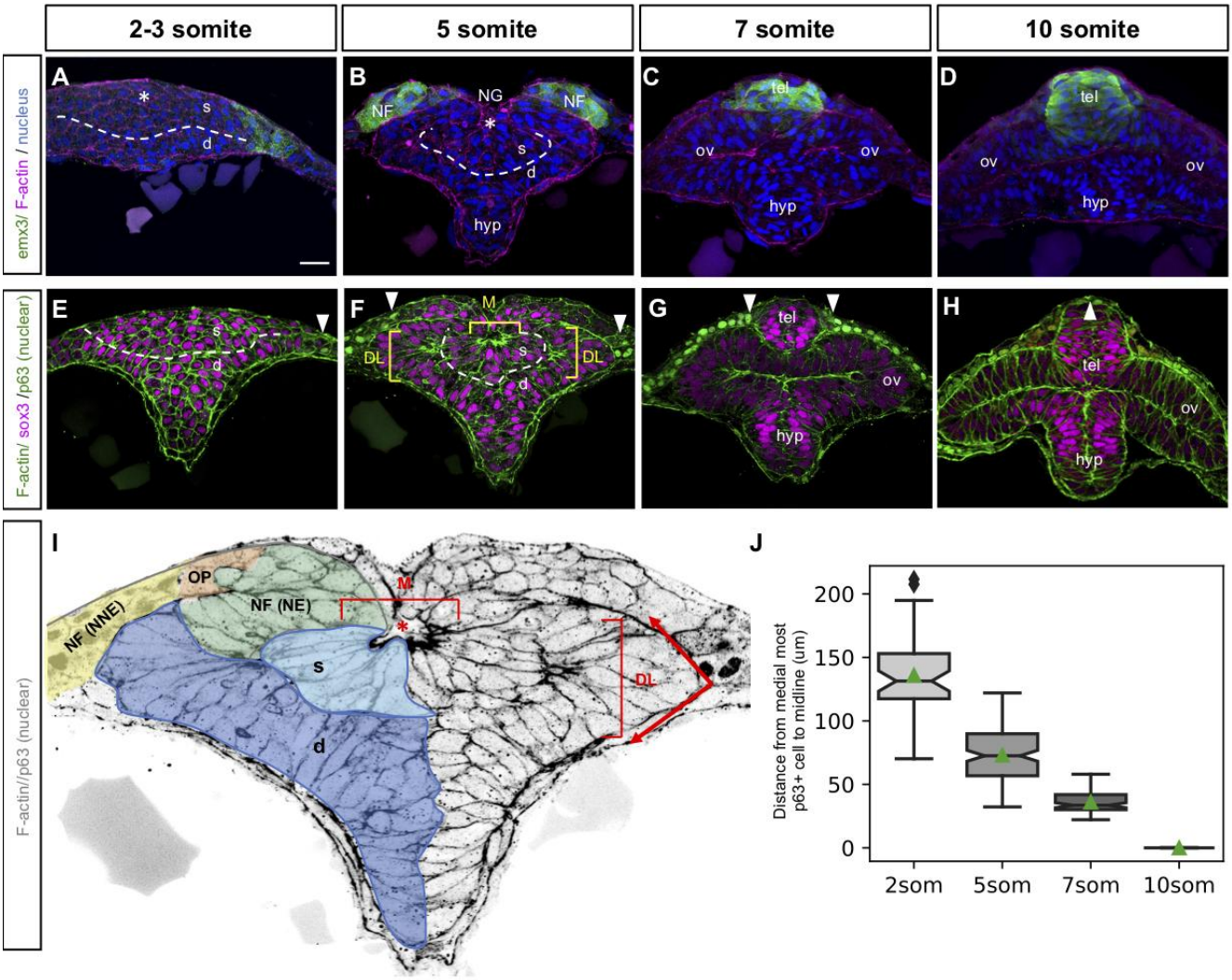

Figure 3. Hingepoints and neural folds contribute to forebrain morphogenesis. (A-D). Transverse sections through the ANP/prospective forebrain of 2-3 som (A, E), 5 som (B, F), 7 som (C, G) and 10 som (D, H) embryos. (A-D) Tg[*emx3:YFP*] embryos labeled with anti-GFP (green), phalloidin (F-actin, magenta) and DAPI (nuclei, blue). (E-H) WT embryos labeled with phalloidin (F-actin, green), anti-Sox3 (magenta) and anti-p63 (nuclear label, green). (I) Higher magnification image of panel F, grey scaled to reveal F-actin and p63 and pseudo-colored on the left side according to cell identity - color code: light blue: superficial eye field cells, dark blue: deep eye field cells that apically constrict to form the optic vesicles, green: neural component of the neural fold, orange: olfactory placode (cells that are Sox3/p63-negative), yellow: non-neural component of the neural fold. (J) Measurement of neural fold convergence, scored as the distance between the medial-most p63-positive cells on either side of the midline at different developmental stages. 2 som: 48 measurements across 14 embryos; 5 som: 144 measurements across 16 embryos; 7 som: 87 measurements across 10 embryos; 10 som: p63 domain is fused, no measurements. Statistical analysis: Mann-Whitney U tests, two-sided; 2 som vs 5 som : P = 1.18e^-21; 2 som vs 7 som : P = 8.35e^-22; 5 som vs 7 som : P = 2.14e^-31. Abbreviations: d = deep layer; DLHP = Dorso-lateral hingepoints; hyp = hypothalamus; MHP = Medial hingepoint; ov = optic vesicle; s = superficial layer; tel = telencephalon. Annotations: double white arrow = placodal cells; white arrowhead = medial-most epidermis; red asterisk = neuropore. All Scale bars: 25 µm.

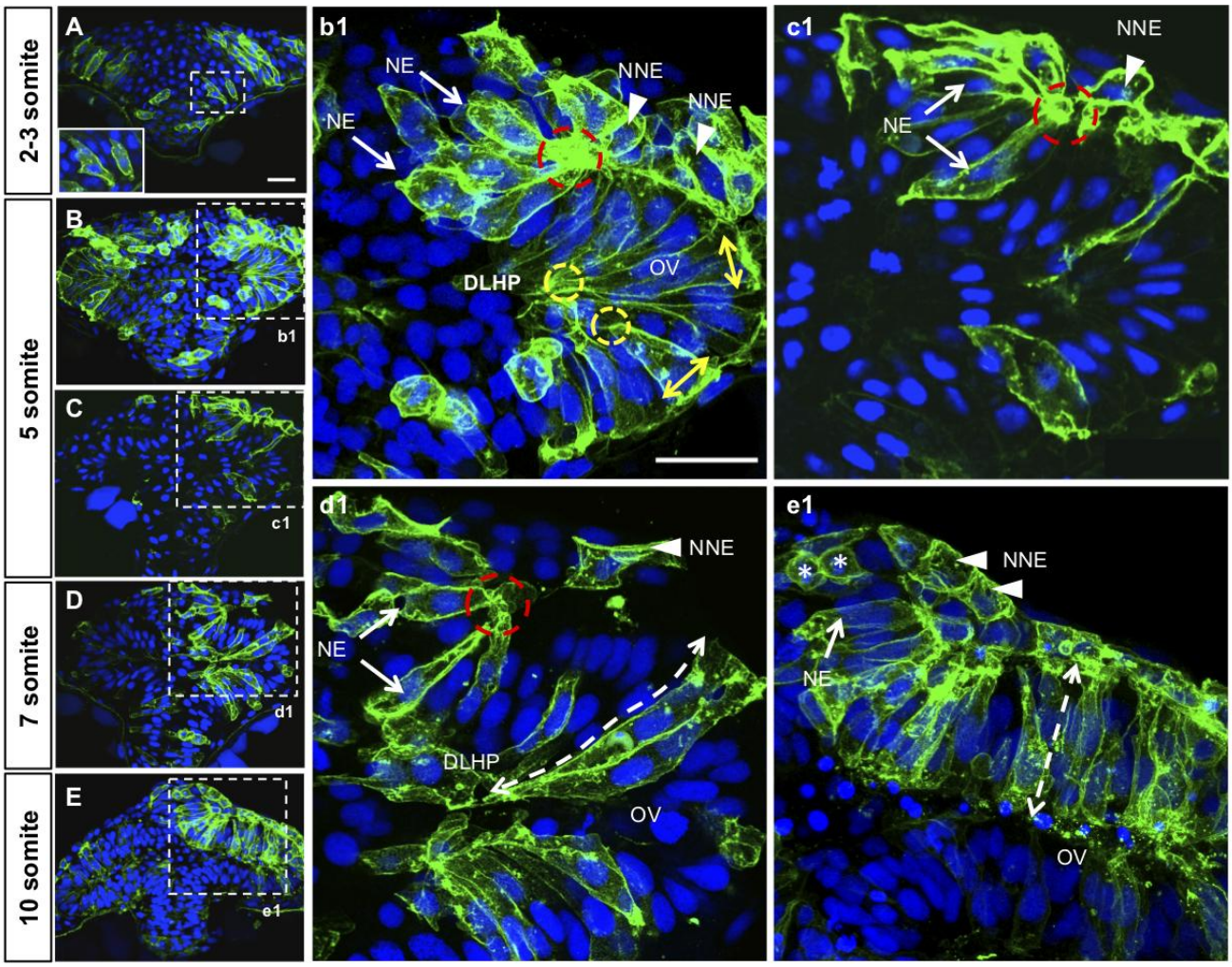

Figure 4. Cell shape changes in the deep layer of the ANP that contribute to DLHP and neural fold formation. (A-E) Transverse section, at the level of the forebrain, of embryos at the 2-3 (A), 5 (B, b1, C, c1), 7 (D, d1) and 10 (E, e1) somite stages mosaically-expressing mGFP (green) and labeled with the nuclear marker DAPI (blue). The inset in A is a higher magnification of dashed area in A**.** (b1-e1) Higher magnifications of regions delineated by dotted lines in (A-E). Annotations: red dashed circle = basal constriction of NE component of neural fold; yellow circle = apical constriction of DLHP cells; arrows = NE component of neural fold; arrowheads = NNE component of neural folds; double dashed arrow = elongated deep cells of the optic vesicle, asterisks = dividing cells in the prospective telencephalon. Scale bars: 25 μm in A and b1.

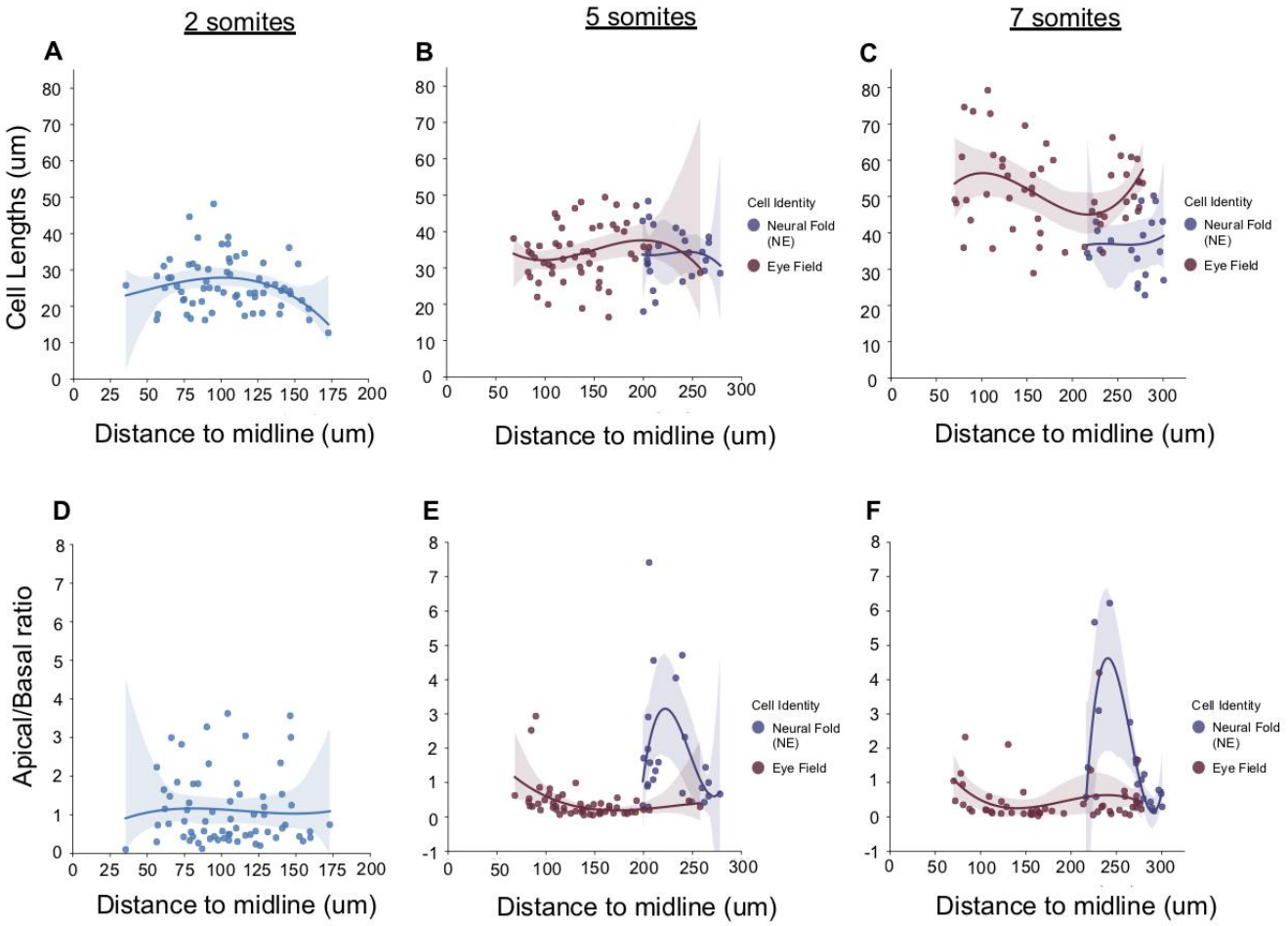

Figure 5. Measurements of cell shape changes in the deep neuroectodermal layer and neural folds. (A-C) Measurements of cell lengths (μM, Y axis) of m-GFP-labeled cells at different positions relative to the ANP midline (μM, X axis). Measurements begin in the region fated to become the optic vesicles. (D-F) Measurements of the apico:basal surface ratio of m-GFP-labeled cells at different positions relative to the ANP midline (μM, X axis). Measurements begin in the region fated to form the optic vesicles. The original scatter plot was fitted to a 3rd degree polynomial. Confidence intervals for the polynomial are 95% and were calculated with 1000 bootstraps. Color code: blue = neuroectodermal cells of the deep layer of 2 som stage embryos that are not yet identifiable based on cellular morphology; red = cells that form the optic vesicles; blue = cells that form the neuroectodermal component of the neural folds.

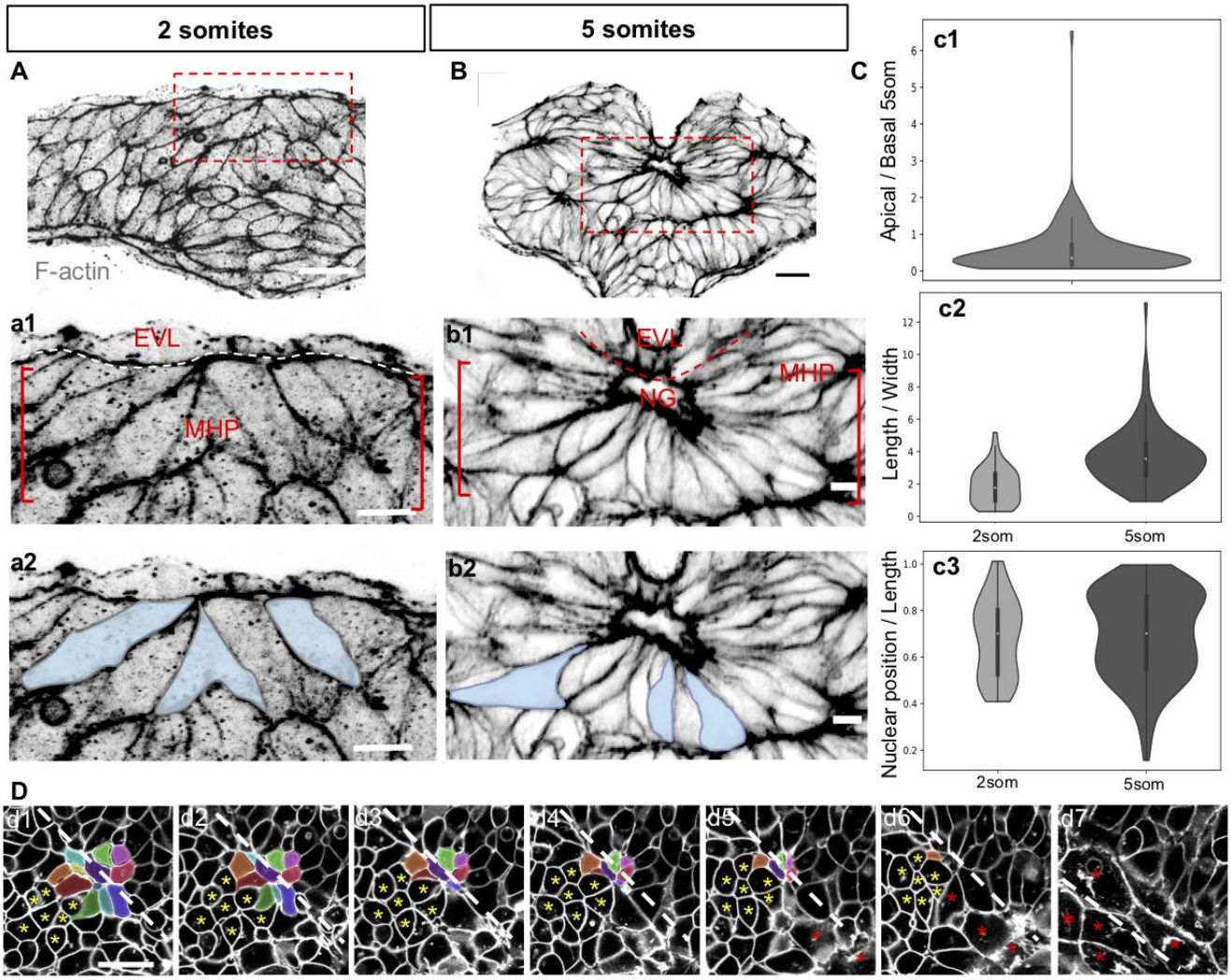

Figure 6. Apical constriction of MHP cells. (A-b2) Transverse sections through the ANP at the 2 (A, a1, a2) and 5 (B, b1, b2) som stages labeled with phalloidin (shown in greyscale). (a1-b2) are higher magnifications of the boxed areas in A and B, revealing the organization of the medial ANP (a1, b1) and the shape of individual MHP cells pseudo-colored in blue (a2, b2). (C) Quantitation of cell shape changes. (c1) Measurements of apical:basal surface ratio. (c2) Measurement of length-to-width (LWR) ratio at 2 som (n= 47 cells from 5 embryos) and 5 som (n= 115 cells from 4 embryos). A Mann-Whitney two-sided U Test revealed that the LWR increase between 2 som and 5 som is statistically significant (P = 7.80e^-11). (c3) Relative position of nucleus at 2 and 5 som measured in the same cell population (c3). Mean nuclear position/cell length of .682 ± .0240 at 2 som vs .696 ± .0174 at 5 som is not statistically significant using a Mann Whitney U test (P= .419). (E) Still frames of time lapse movie of m-GFP labeled embryo imaged from a dorsal view. Individual MHP cells are pseudo-colored, A cluster of cells adjacent to the MHP is indicated with yellow asterisks and EVL cells are labeled with red asterisks . Abbreviations: EVL = enveloping layer; MHP = medial hingepoint; NG = neural groove. Annotations: asterisk = medial groove; brackets = MHP region. Scale bars: 25 µm in A and B, 10 µm in a1, a2, b1, b2, d1.

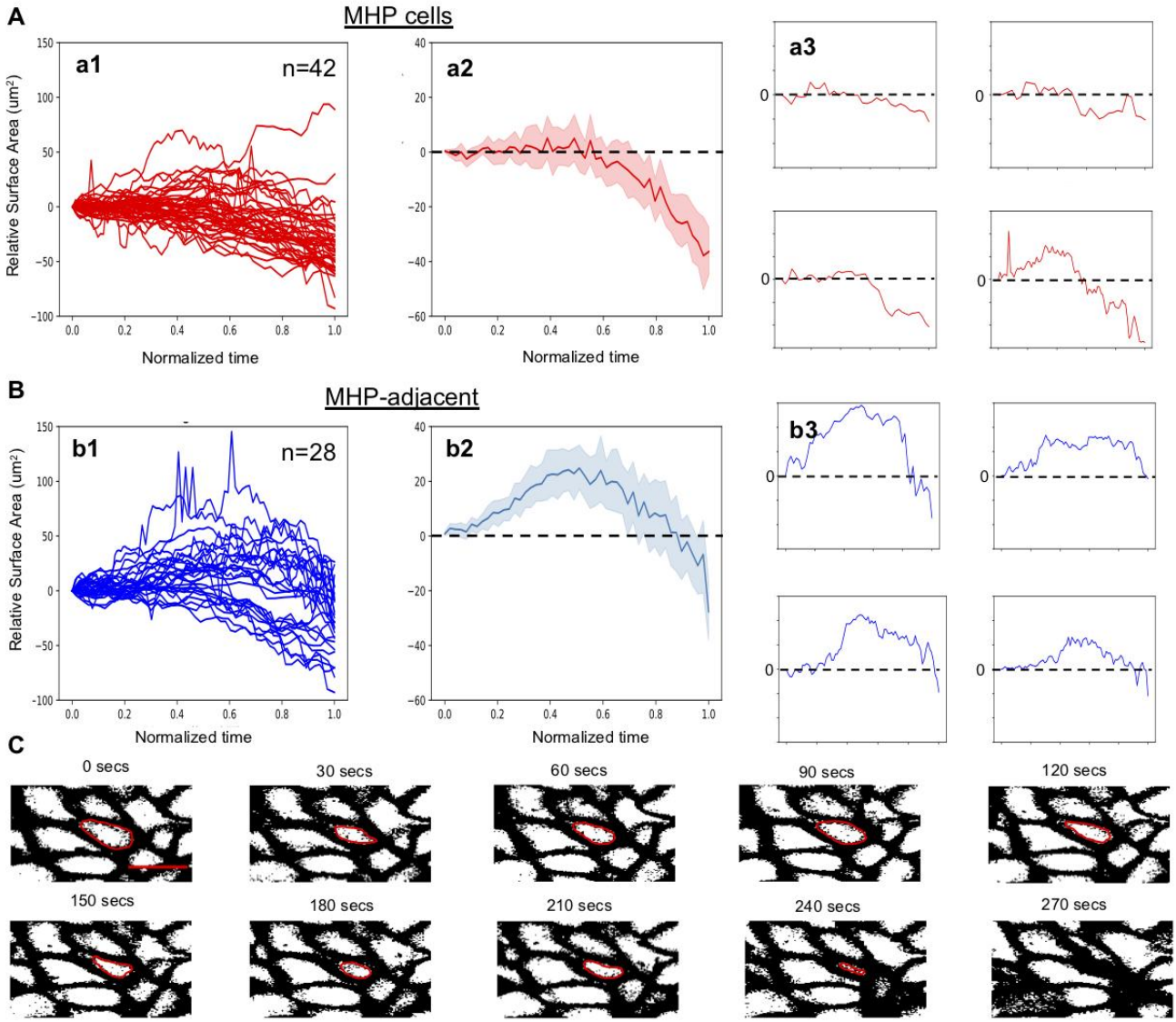

Figure 7. Oscillatory constriction with decreasing amplitude reduces the apical surface of MHP cells. (A) Measurements of medial, MHP cells. (a1) Relative apical surface areas over time for individual MHP cells. (a2) Mean values of MHP relative apical surface areas over time, 95% confidence interval. (a3) Representative traces of relative apical surface areas over time for individual MHP cells**.** (B) Measurements of MHP-adjacent cells. (b1) Relative apical surface areas over time for individual MHP-adjacent cells. (b2) Mean values of MHP-adjacent relative apical surface areas over time, 95% confidence interval. (a3) Representative traces of relative apical surface areas over time for individual MHP-adjacent cells. (C) Still frames of time-lapse movie of m-GFP labeled cells shown in grey-scale. The oscillatory behavior of one cell, outlined in red, is shown over time. Scale bar: 10 μm in c1.

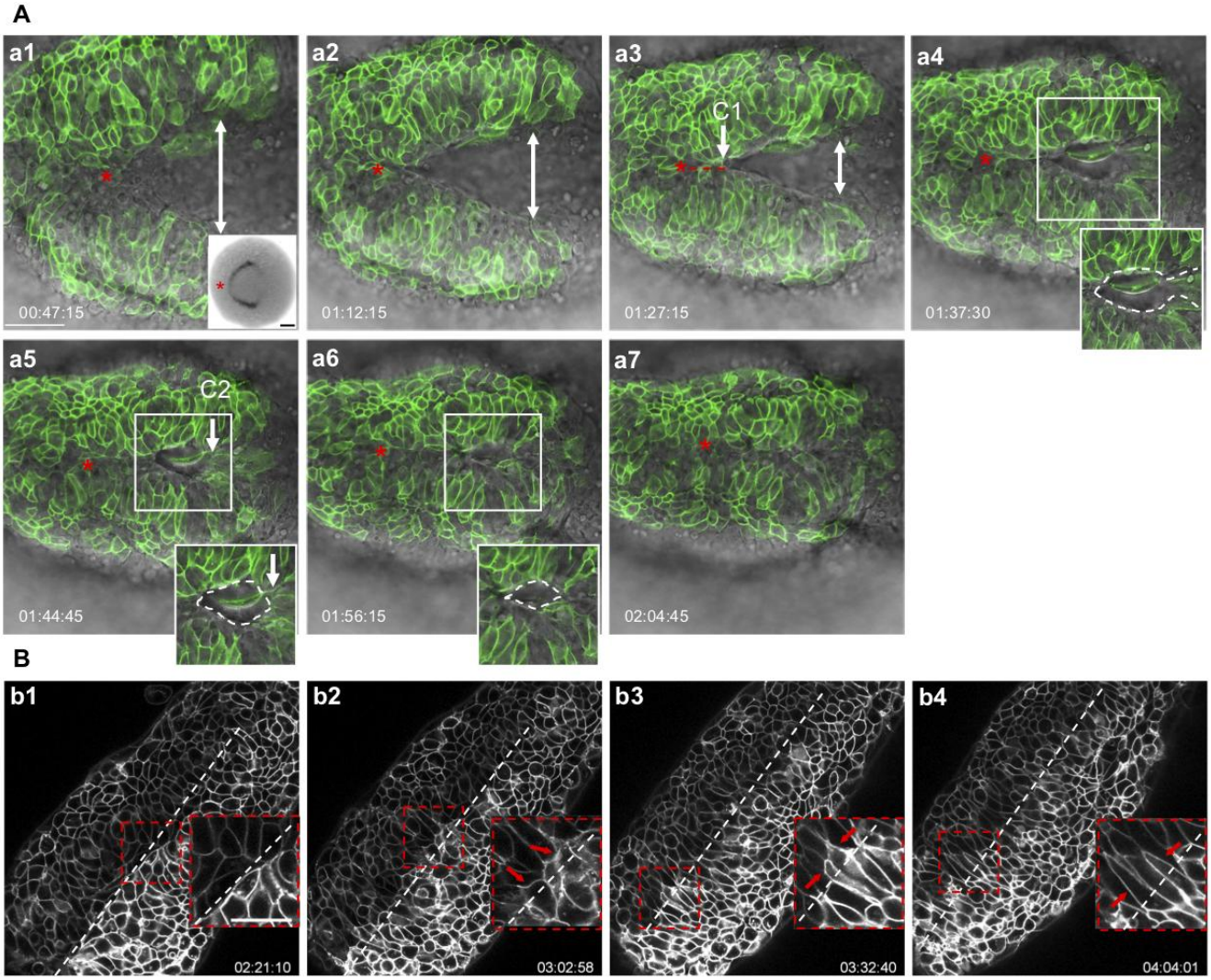

Figure 8. Dynamics of neural fold fusion. (A, a1-a7) Time lapse movie frames of an embryo expressing mosaic GFP, imaged from a dorsal view, showing the initiation of neural tube closure. Images are overlays of the green and brightfield channels. Inset in a1 shows a dorsal view of an *emx3*-labeled embryo. Insets in a4-a6 outline the eye-shaped opening that forms between closure sites one (CP1) and two (CP2) (B) Grey-scale time-lapse movie frames of an mGFP-labeled embryo imaged from a dorsal view, revealing the final stages of neural fold fusion. Insets in the lower right corner of panels b1-b4 are higher magnification views of boxed areas. Abbreviations: C1, C2: closure sites one and two. Annotations: red asterisk: apex of the neural fold arc; red dotted line: synchronous and posteriorly-directed neural fold fusion anterior to closure point one; white double arrows: distance between the neural folds; white dotted oval: eye shaped opening, the corners of which are defined by closure points one and two; white dotted line: embryonic midline; red arrows: filopodia extending across the midline; time-elapse is shown at the bottom of each panel.Scale bars: 50 μm in a1, 100 μm in a1 inset, and 25 μm in b1.

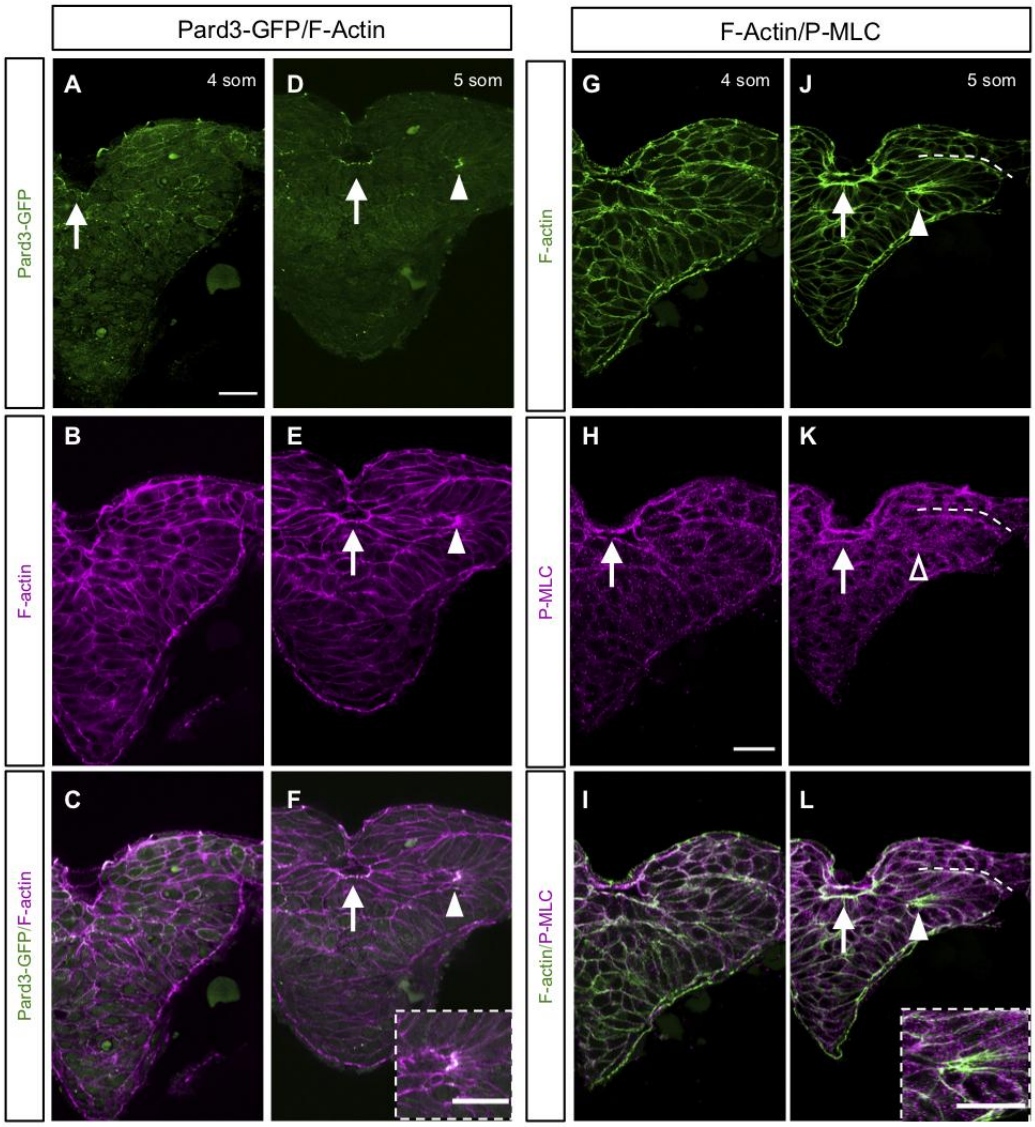

Figure 9. Molecular characterization of the MHP. (A-L). Transverse sections through the ANP at the 4 (A-C, G-I) and 5 (D-F, J-L) som stages. (A-F) Embryos double-labeled with Pard3-GFP (green) and phalloidin (F-actin, red) (G-L) Embryos double-labeled with anti-P-MLC (red) and phalloidin (F-actin, green).(C, F, I, L) Magenta and green channel overlay. Insets in F and L show higher magnification images of the DLHP. Annotations: arrow = MHP; arrowhead = DLHP; dotted line (in J-L) = interface between the NE and NNE layers of the neural folds. Scale bars 25 μm.

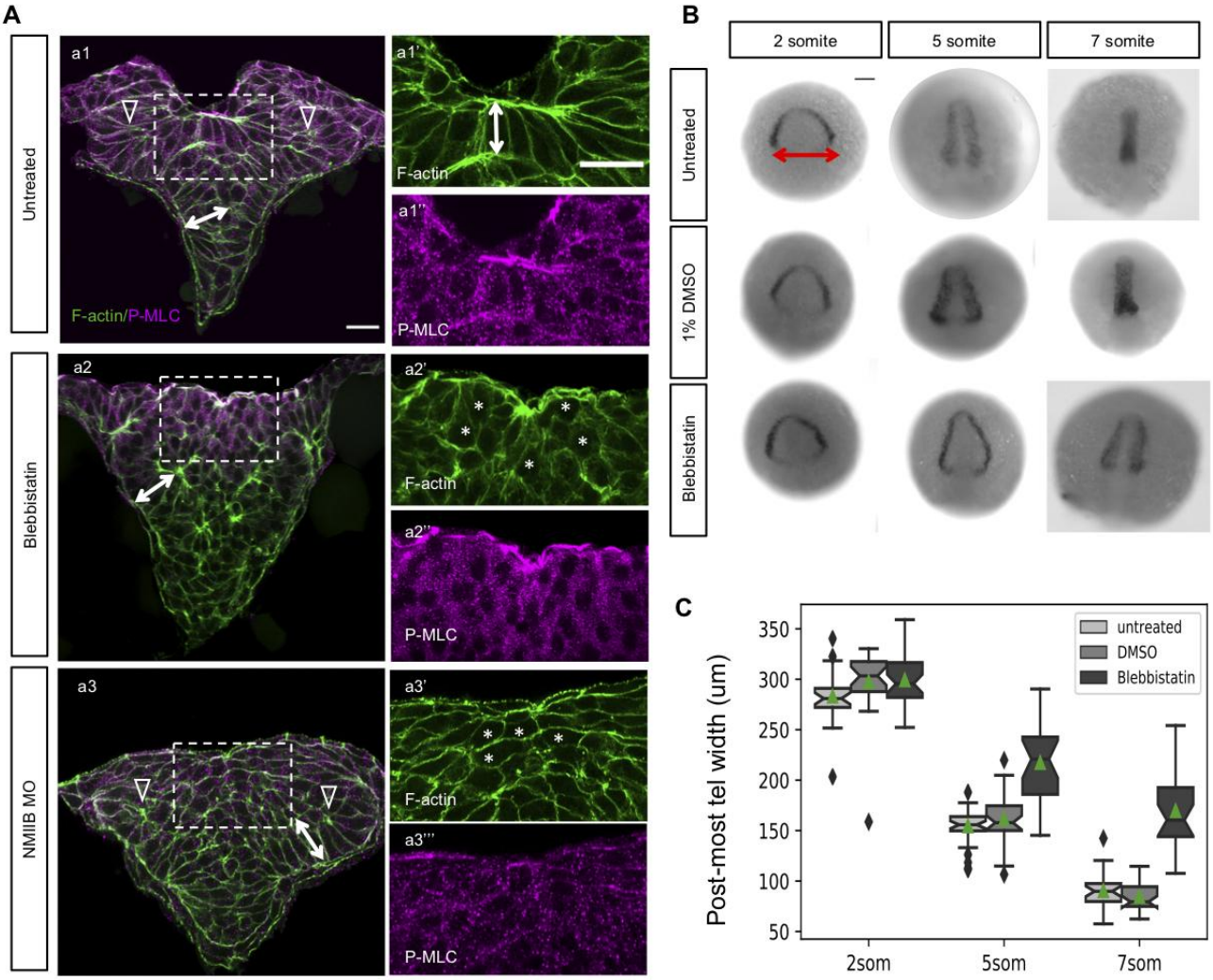

Figure 10. Role of non-muscle myosin II in apical constriction and neural fold convergence. (A). Transverse sections through the ANP of 5 som control, untreated (a1-a1''), blebbistatin-treated (a2-a2'') and *NMIIB* MO-injected (a3, a3', a3''). Embryos were double-labeled with phalloidin (F-actin,green) (A-F) and anti-P-MLC (red). (B) Dorsal views of 2, 5 and 7 som embryos untreated (top panels), DMSO-treated (middle row) and blebbistatin-treated (bottom row) labeled via *in situ* hybridization using an *emx3* riboprobe. (C) Boxplots showing distribution of posterior-most telencephalon widths (double red arrow in B) according to treatment group. Line in the middle of each boxplot is the median, notches around the median are 95% confidence intervals. Green triangles show the means. At least two independent experimental trials were performed for each developmental stage and treatment group. 2 som: Untreated: n=26, mean=283.224 ± 5.18; DMSO-treated: n= 26, mean=297.727 ± 6.41; blebbistatin-treated: n = 34, mean=299.412 ± 4.40. 5 som: Untreated: n=33, mean=154.688 ± 3.174; DMSO: n=30, mean=161.747 ± 4.73; blebbistatin-treated: n=23, mean=217.472 ± 8.43. Two-sided Mann Whitney U test: 5 som untreated vs DMSO: P=0.332; 5 som untreated vs blebbistatin-treated: P=1.30e^-7; 5 som DMSO-treated vs blebbistatin-treated: P = 3.50e^-6. 7 som: untreated: n=28, mean=90.444 ± 3.31; DMSO-treated: n=27, mean 84.855 ± 2.88; blebbistatin-treated: n=24, mean= 169.779 ± 7.52. Two-sided Mann Whitney U test: 7 som untreated vs DMSO: P=.170; 7 som untreated vs blebbistatin-treated: P=2.06e^-9; 7 som DMSO-treated vs blebbistatin-treated: P = 1.46e^-9. Annotations: double white arrows = cell length in deep layer; open arrowhead = DLHP; asterisks = rounded neuroectodermal cells; red double arrow = posterior-most telencephalon width. (a1'-a3'') Higher magnifications of boxed in areas in a1-a3. Scale bars: 25 µm in a1; 25 µm in a1' and 100 µm in B.

SUPPLEMENTARY FIGURE LEGENDS

Supplemental Figure 1. 3-Dimensional rotation revealing organization of neural fold cells in a 5 som embryo. Transverse section, at the level of the forebrain of a 5 somite embryo mosaically-expressing mGFP.

Supplemental Figure 2. 3-Dimensional rotation revealing organization of neural fold cells in a 7 som embryo. Transverse section, at the level of the forebrain of a 7 somite embryo mosaically-expressing mGFP.

Supplemental Figure 3. MHP cells undergo oscillatory constriction with decreasing amplitude. Time lapse imaging of embryo ubiquitously expressing mGFP. Clusters of medial (MHP) constrict apically in an oscillatory manner, in contrast to their lateral neighbors that do not. Annotations: cyan dots = MHP cells; yellow asterisks = MHP-adjacent cells that do not undergo apical constriction, yellow dashed line: midline, red asterisks = EVL cells.

Supplemental Figure 4. Neural tube closure is initiated at two closure points in the forebrain. Time lapse imaging of embryo mosaically-expressing mGFP. The Green and brightfield channels are overlaid to reveal the shape of the neural folds and neural groove. Annotations: red asterisk: apex of the arch shaped neural folds; white dotted line: contour of the eye-shaped opening whose corners are defined by closure points 1 and 2, double headed arrow: width of the neural plate, which decreases over time, white arrows: closure points 1 and 2, respectively.

Supplemental Figure 5. Neural fold cells extend filopodial protrusions across the midline. Time lapse imaging of embryo ubiquitously expressing mGFP. Cells (cyan and magenta) originating from contralateral sides of the ANP extend medially-oriented filopodia and transiently interdigitate across the midline (yellow dashed line).